ACS APPLIED MATERIALS & INTERFACES

Research Article

www.acsami.org

Dynamic Optical Gratings Accessed by Reversible Shape Memory

Cary A. Tippets,[†,⊥] Qiaoxi Li,[‡,⊥] Yulan Fu,[§] Eugenii U. Donev,[§,∥] Jing Zhou,[‡] Sara A. Turner,[‡] Anne-Martine S. Jackson,[‡] Valerie Sheares Ashby,[‡] Sergei S. Sheiko,*[,‡] and Rene Lopez*[,§]

[†]Department of Applied Physical Sciences, University of North Carolina at Chapel Hill, Chapel Hill, North Carolina 27599, United States

[‡]Department of Chemistry, University of North Carolina at Chapel Hill, Chapel Hill, North Carolina 27599, United States

[§]Department of Physics and Astronomy, University of North Carolina at Chapel Hill, Chapel Hill, North Carolina 27599, United States

Supporting Information

ABSTRACT: Shape memory polymers (SMPs) have been shown to accurately replicate photonic structures that produce tunable optical responses, but in practice, these responses are limited by the irreversibility of conventional shape memory processes. Here, we report the intensity modulation of a diffraction grating utilizing two-way reversible shape changes. Reversible shifting of the grating height was accomplished through partial melting and recrystallization of semicrystalline poly(octylene adipate). The concurrent variations of the grating shape and diffraction intensity were monitored via atomic force microscopy and first order diffraction measurements, respectively. A maximum reversibility of the diffraction intensity of 36% was repeatable over multiple cycles. To that end, the reversible shape memory process is shown to broaden the functionality of SMP-based optical devices.

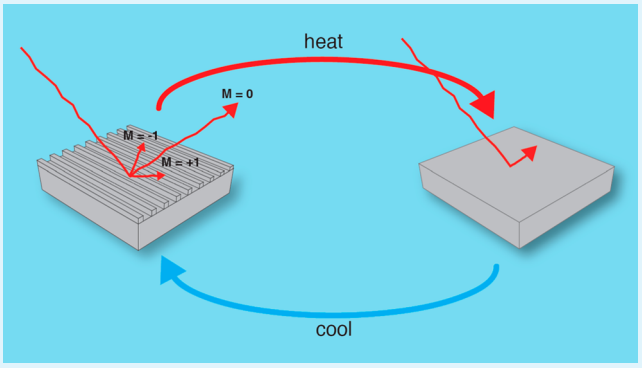

KEYWORDS: *shape memory polymers, reversible shape memory, responsive surfaces, photonic structures, elastomers*

INTRODUCTION

Technological advances increasingly require optical components to be adaptable and multifunctional. Standard photonic components are typically crafted from rigid materials, with photonic structures often fabricated using ruling processes and copied with other rigid materials.[1] This rigidity allows photonic components to have only a single designed function, while in some cases, switchable micro-optics components are desirable. Advances in soft lithography have allowed for the production of adaptable optical elements that use polydimethylsiloxane (PDMS) elastomers to mold photonic shapes.[2−5] These photonic replicas can be stretched or compressed to induce a tunable optical response and thus have shown a promising ability for use in optical setups, but the need for constant loads to be applied limits the application of these devices.

Shape memory polymers (SMPs) are polymer networks capable of switching from one programmed shape to another. Two programming steps are necessary to prepare a semicrystalline elastomer for shape memory actuation. First, an original (primary) shape is obtained via physical or chemical cross-linking.[6] The temporary (secondary) shape is then programmed by heating the cross-linked sample above its melting temperature (T_m), applying a force, and cooling below T_m with the force still in place. When the force is removed, the secondary shape is maintained until a suitable external stimulus of heat, sound, light, or electricity is applied.[7−10] However, without external forces or designed structural constrains, most shape memory processes are irreversible.[11−13] Recent studies have shown that it is possible to reversibly "shape-shift" between two programmable shapes without applying external forces or reprogramming in a process called reversible shape memory (RSM). This approach offers a new route to hands-free multifunctionality[14−16] and is a consequence of the interplay of the crystalline scaffold and chemical cross-links, which are each capable of encoding a distinct shape. Partial melting of the crystalline scaffold leaves behind a latent crystalline template, and the programmed shape is recovered upon cooling by self-seeded crystallization along kinetically preferred pathways to replicate the scaffold. The reversibility is controlled by tuning the chemical cross-linking density and the partial melting temperature. At a macroscopic scale, the maximum reversibility of tensile strain has been reported as 75% for poly(octylene adipate) elastomers.[14]

Compared to rigid optical components, SMP optics can be tunable with no external force needed to maintain a secondary shape. At smaller scales, SMPs have been explored for their ability to memorize micrometer and sub-μm features as well.[17−19] For example, Xu et al. crafted deformable micro-

Received: March 27, 2015
Accepted: June 17, 2015
Published: June 17, 2015

DOI: 10.1021/acsami.5b02688
ACS Appl. Mater. Interfaces 2015, 7, 14288−14293

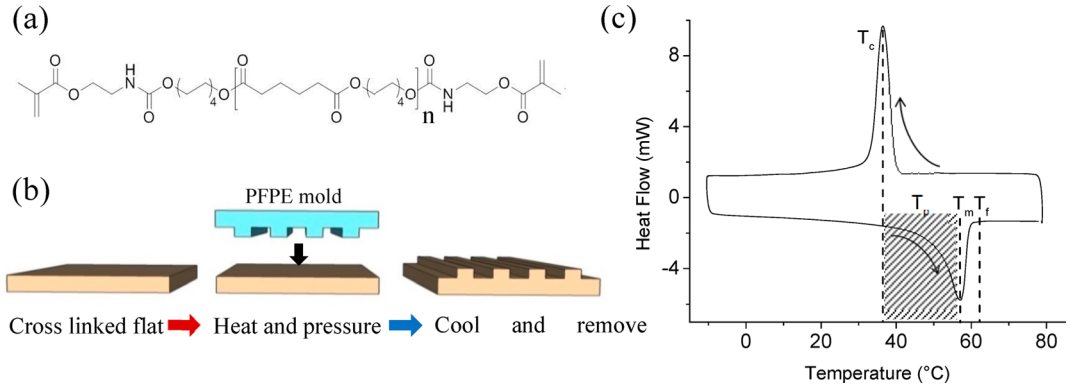

Figure 1. (a) Chemical structure of methacrylate-terminated poly(octylene adipate) (n = 13). (b) The molding process: a glass slide is used to cure an optically flat surface of poly(octylene adipate). A 750 nm pitch perfluoropolyether (PFPE) grating is used as a mold to emboss the heated flat surface. After cooling, the mold is removed, and the grating structure remains on the SMP surface. (c) A differential scanning calorimetry (DSC) thermogram of a cross-linked POA sample indicates the temperature range of partial melting temperatures (T_p, hatched region), the melting peak (T_m = 58 °C), the temperature of complete melting (T_f = 64 °C), and the crystallization peak (T_c = 37 °C) (arrows indicate ramping direction).

optic surface structures from SMPs for use as dynamic optical components.[17] However, the advantages of SMP micro-optics are often hampered by the irreversibility of most shape memory processes. Previous studies have demonstrated that micro-structured surfaces can be modulated via RSM to change surface effects including adhesion and wetting.[18]

Here, we report on the utilization of RSM at a sub-μm scale to create a reversibly tunable optical element. The ridge-type grating was chosen as a simple proof-of-principle model due to the straightforward relationship between ridge height and diffraction intensity. Understanding the reversible behavior of this photonic structure can then be extended to other grating geometries, for example, tooth-shaped,[20] sawtooth shaped,[21] and triangle shaped.[22] We have programmed a sub-μm ratio optical grating that exhibits reversible magnitude changes of its diffraction intensity (up to about 36% modulation) when subjected to alternating changes in temperature. We have verified that this result is attributable to reversible modulation in the grating's ridge height and that it is repeatable over multiple cycles. By melting all crystalline regions within the sample, the grating structure can be erased, recovering the primary flat surface, which can then be reprogrammed to a new shape.

EXPERIMENTAL SECTION

Material Fabrication. For this experiment we sought to fabricate the reversible optical element in a representative semicrystalline polymer poly(octylene adipate) (POA) as reported previously.[14] The chemical structure of end-functionalized POA is shown in Figure 1a. To utilize the best RSM behavior of POA, we synthesized POA with a number-average degree of polymerization (DP) of n = 13 (M_n = 3500 g/mol), which is known to exhibit significant shape reversibility.[14] In the previous work, we used the condensation polymerization between adipic acid and octylene diol to produce POA,[14] while in the present study, we have improved this synthesis by adipoyl chloride reacting with octylene diol. The new route provided a faster reaction and more accurate control of molecular weight distribution. This resulted in a higher T_m of 58 °C, compared to that of the previous synthesis, which was around 50 °C. Under the experimental ramping condition, a strain reversibility of 41% was observed when the shape-memory polymer was subjected to 15% uniaxial strain deformation (Figure S1, Supporting Information). Figure 1b displays a two-step thermosetting procedure that has been used to make an optical grating with reversible control over grating height. First, POA was mixed with 10 wt % $CHCl_3$ and 1 wt % 2,2-diethoxyacetophenone. The mixture was then injected into a Teflon mold, covered with a glass slide, and cross-linked with 365 nm UV light for 5 min. This produced a RSM substrate with an optically flat surface as the primary shape. The substrate was then annealed free-standing at 70 °C overnight to extract the remaining solvent and thermal history. Next, the substrate was heated to 70 °C, and the optically flat surface was pressed against a perfluoropolyether (PFPE) grating (pitch, 750 nm; ridge height, 250 nm; ridge width, 250 nm) followed by quenching in an ice bath. On separation of the substrate and the PFPE mold, the surface was in its secondary grating shape, which accurately replicated the PFPE grating.

Optical Measurements. Experimental measurements of the grating diffraction intensity were taken under illumination using light from a 633 nm He−Ne laser, which was incident at a 5° angle with respect to the sample normal; the experimental set up is shown in Figure S2 (Supporting Information). The 750 nm grating pitch was chosen, such that only the M = +1 diffraction order will be measured, with sufficient angular space between the specular reflection (M = 0). Planar diffused silicon photodiodes (United Detector Technology) with a spectral sensitivity from 400 to 1100 nm and a responsivity of ~0.4 A/W at 633 nm were used to monitor the intensity of the first-order diffraction mode and the intensity of the incident beam in order to correct for power fluctuations. Incident beam intensity was monitored by splitting the initial beam with a 50/50 beam splitter. Simultaneously, the first-order diffracted light was monitored, and relative intensity was calculated by normalizing the diffracted beam intensity with the incident beam intensity. The temperature of the sample was controlled using a thermoelectric stage and a thermocouple directly in contact with the sample surface. To achieve RSM performance, instead of complete melting, we brought the POA gratings to a partial melting temperature (T_p; Figure 1c) at a heating rate of 1 K/s, and then held for at least a minute before natural cooling at a slower rate dictated by the thermal equilibration at room temperature (RT).

RESULTS AND DISCUSSION

Microscopic and Morphological Characterization. Temperature-triggered variations of the grating topography were monitored in situ using an atomic force microscope equipped with a heating−cooling stage. In previous work, the maximum reversibility of POA was achieved when the partial melting temperature T_p was close to the melting peak T_m.[14] In the present work, we have therefore recorded AFM measurements for the same maximum reversibility cycle ranging from RT to T_p = 56 °C. The ridge height was found to vary with temperature, while all other grating parameters remained constant. Figure 2a−c shows the first heating−cooling cycle from an as-prepared grating structure, Figure 2d,e shows the

DOI: 10.1021/acsami.5b02688
ACS Appl. Mater. Interfaces 2015, 7, 14288−14293

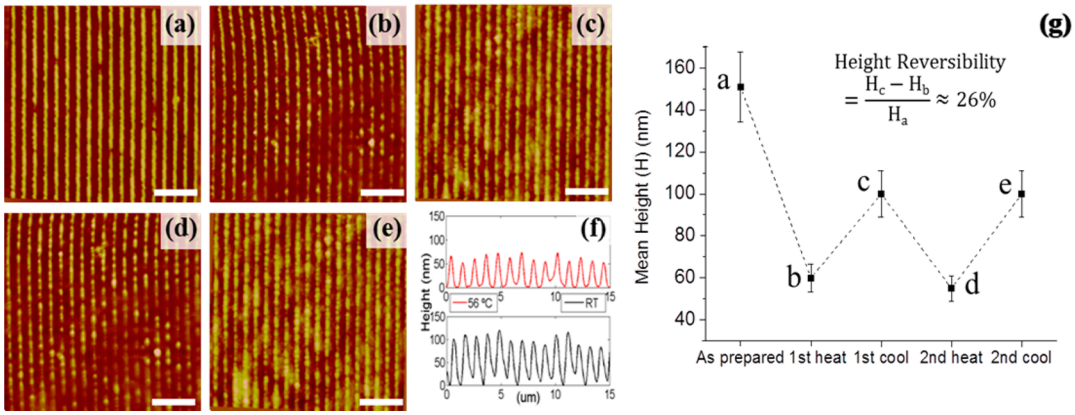

Figure 2. AFM images (a) as prepared and at room temperature, (b) after heating to 56 °C at 1 K/s, and (c) after cooling back to room temperature. (d) Second heating to 56 °C at 1 K/s and (e) after subsequent cooling back to room temperature. All scale bars are 5 μm. (f) Height averaged line profile of the sample during one heating cycle (top) at 56 °C and (bottom) cooled to RT. (g) The corresponding AFM mean ridge height was averaged over 180 line profiles per AFM image. The height reversibility is calculated using the mean heights of corresponding AFM images.

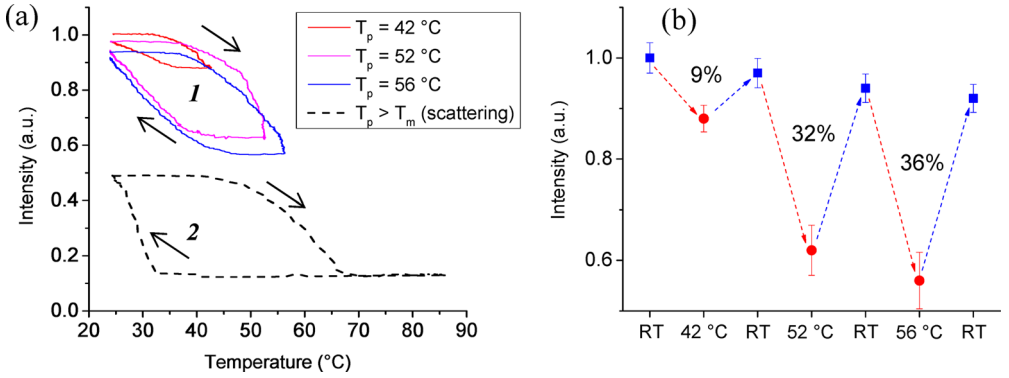

Figure 3. (a) Optical intensity of a diffraction spot as temperature was varied (arrows showing ramping direction). Region 1: Optical intensity can be reversibly controlled within different cycles with T_p kept below T_m. Region 2: When T_p is increased above T_m, the grating is greatly erased and nonrecoverable. The intensity drops significantly as the temperature increases to T_f (T_f = 70 °C). Now the surface returns to its flat primary shape and the intensity changes upon cycling are due to melting/crystallization-induced scattering. (b) Optical reversibility was calculated for three T_p cycles. A maximum optical reversibility of 36% was achieved when T_p was set at 56 °C, which is close to T_m.

second heating−cooling cycle, indicating good repeatability. Average line profiles of the sample at 56 °C and after cooling to RT are shown in Figure 2f. Average ridge height analysis (Figure S3, Supporting Information) of the line profiles shows the height reversibility is around 26% (Figure 2g). This microscopic reversibility of the grating feature is less than the bulk reversibility (~41%) of a polymer film when subjected to 15% uniaxial strain deformation. The discrepancy between bulk and microscopic reversibility may be due to plastic deformation and crystallization. We ascribe the observed plastic deformation to the nonuniform strain distribution generated by the embossing process used for shape programming, which possibly induced the nonerasable grating artifacts present in a few locations even after complete sample melting (Figure S4, Supporting Information). In addition, we know from previous work that freshly molten chains tend to recrystallize into large spherulites (~10 μm),[14] which interfere with crystallization in the nanoscale confinement of the grating and lead to a rough surface structure.

Reversible Optical Properties. Variations in the optical properties of the RSM grating due to the observed change in surface topography were explored. Figure 3a depicts a reversible change in diffraction intensity upon the corresponding variation in substrate temperature (Figure 1a, Region 1). Before reaching 40 °C, the change in intensity is minimal. This finding agrees with the previous results indicating that the onset of shape recovery occurs only after melting of at least ~10 wt %/wt of the initial crystallinity.[14] Above 40 °C, the diffraction intensity begins to decrease due to the onset of shapeshifting (Figure 4b). Upon continued heating to a partial melting temperature T_p = 42 °C, the diffraction intensity continues to decrease. Upon cooling, the intensity recovers toward its initial value at RT (Figure 4a), indicating good optical reversibility (Figure 3b). When a POA grating is heated to a higher temperature (T_p = 52 or 56 °C), the observed intensity modulation increases as well (Figure 3b). For each T_p, we heated and cooled a single POA grating sample multiple times between RT and T_p, and observed that the intensity change was repeatable over multiple cycles. Typical experiments included 2−3 cycles per temperature, with less than 5% variation in optical intensity. Further cycling at a single T_p resulted in a loss of ~10% of optical intensity over 25 cycles. In Figure 3a, only one cycle for each T_p is shown for clarity. By varying T_p, we located the optimal melting temperature to maximize reversibility: The maximum optical reversibility is ~36% and is found when partial melting T_p = 56 °C, which is near the T_m (Figure 1c), and is consistent with the previous RSM study.[14] As we explain later, when a

DOI: 10.1021/acsami.5b02688
ACS Appl. Mater. Interfaces 2015, 7, 14288−14293

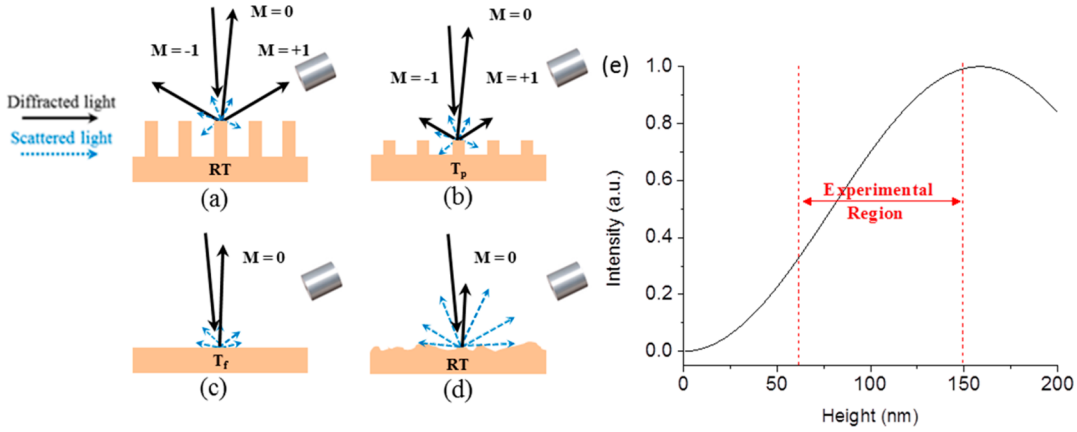

Figure 4. Diffraction and scattering intensity change with temperature. The first diffraction order was monitored as the grating was (a) cooled to RT and (b) heated to a partial melting temperature T_p. Arrow length indicates relative intensity, which relates to grating height. (c) At T_f, the surface returns to optically flat, the detector only picks up scattering signal, and (d) when cooled back to RT, crystals form in an unrestricted fashion, resulting in an optically rough surface that more readily scatters light. (e) Theoretical calculations indicate a sine-squared relationship between grating height and grating efficiency between 10 and 200 nm. As grating height decreases from ~150 to 60 nm, the measured intensity should decrease in near linear fashion.

sample is heated to $T_p > T_m$, the grating is largely erased and the shapeshifting process is nonreversible.

The optical reversibility (OR; Figure 3b) is calculated as:

$$\mathrm{OR} = \frac{I_{\mathrm{RT,end}} - I_{T_p,\mathrm{partial\ melt}}}{I_{\mathrm{RT,start}}} \quad (1)$$

where $I_{\mathrm{RT,start}}$ is the intensity of diffracted light (first diffraction order) by the grating at room temperature before heating; $I_{T_p,\mathrm{partial\ melt}}$ is the intensity of the diffracted light at a temperature of partial melting (T_p); $I_{\mathrm{RT,end}}$ is the intensity after cooling back to room temperature. The first diffraction order was measured at 68° from the grating normal, and it was more than 10 times brigther than light detected in other directions due to some minor random scattering. Therefore, the observed optical reversibility is mainly attributable to changes in height of the grating ridges as a result of the RSM behavior. As the temperature increases, a sufficient fraction of crystalline scaffold has melted, which causes the grating to return toward its flat primary shape. Within the range $T_p < T_m$, enough crystallites remain to recover the embossed secondary shape upon cooling through self-seeded recrystallization, and the diffraction efficiency shows excellent reversibility and good repeatability over multiple cycles. Therefore, by referring to T_m as an upper temperature and lower grating height limit, a proper programing protocol can be determined for a desired reversible photonic actuation. The intensity never returns completely to the as-prepared programmed shape due to partial relaxation of the chemical network during recrystallization after each heating−cooling cycle. Note that the strained chemical network always tends to return to its equilibrium unperturbed state (primary shape).[9,14] However, the natural trend of thermodynamic equilibration is reversed by the kinetics of recrystallization of the constrained network strands, which is biased by the remaining crystallites carrying the memory of the programmed secondary shape.

When $T_p > T_m$, the POA grating enters a new behavior regime 2 (Figure 3a). In this regime, a majority of the crystallites have melted, allowing the chemical network to relax to its thermodynamically preferred shape dictated by the chemical cross-links and causing the sample to return toward its flat, primary shape. Upon heating to 85 °C, the grating is largely destroyed and nonrecoverable with only some small residues of grating structure (less than 10 × 10 μm over a 50 × 50 μm scan window; Figure S4, Supporting Information) and the surface returns to its original flat morphology. The optical intensity drops to a minimum value dictated by intrinsic scattering in the substrate.

Separation of Diffraction and Scattering. In Figure 3a Region 2, the optical response appears to be comparable in magnitude to that of Region 1, but the distribution of the detected light is different for both regions. In Region 2, the sample has been heated beyond T_m, and the periodic grating is completely destroyed, so the majority of the light is simply reflected by a flat melted surface in a specular fashion, missing the detector still located where the first diffraction order used to propagate (Figure 4c). When the sample is cooled from its fully melted state, the intensity increases when T_c = 37 °C is reached, and the sample undergoes a random crystallization without trace of any shape memory effect. This random crystallization gives rise to pronounced light scattering in all directions, including that of the detector (Figure 4d). As the surface becomes optically rough, the light that was previously diffracted and specularly reflected now contributes to the scattered light. Intensity contributions from residual grating due to plastic deformation are minor, as the areas are randomly distributed over the entire sample and constitute a small percentage of surface (<10%). It should be noted that this behavior is in distinct contrast with the modulation in Region 1, where the grating exists at all times and the bulk of the detected light is the first diffraction order with a minimal contribution from scattered light (<10%) (Figure S5, Supporting Information). We have conducted a separate study to distinguish individual contributions from diffraction and scattering while a grating is present (Figure S5, Supporting Information). The random scattering contribution in Region 2 is due to polymer crystallization yielding a heterogeneous assembly of randomly oriented crystallites with a size distribution ranging from 10 to 1000 nm. This resulted in isotropic scattering, with minor variances of 1−2% observed. This result may offer an alternative way to study crystallization-induced surface roughness.

DOI: 10.1021/acsami.5b02688
ACS Appl. Mater. Interfaces 2015, 7, 14288−14293

Theoretical Diffractive Mode Intensity. The magnitude of the diffraction intensity change can be understood by analyzing the effect of the grating height. When a monochromatic laser beam is incident on a reflective diffraction grating surface, the reflected light interferes in a phase-sensitive manner that depends on the grating spacing, height, and overall geometry and produces a series of bright diffraction modes. For an ideal diffraction grating, the intensity of zeroth- and first-order diffraction modes can be represented by eqs 2 and 3, respectively.[23]

$$I_0 \propto \cos^2(2\pi\delta/\lambda) \quad (2)$$

$$I_1 \propto \sin^2(2\pi\delta/\lambda) \quad (3)$$

where δ is the height of the grating, and λ is the wavelength of the laser beam. Figure 4e shows that the diffraction efficiency of the first order diffraction mode increases with the grating height monotonically when the height is below 160 nm, which offers a wide operation range for a possible application. When the RSM grating is heated, its ridges decrease in height, reflecting weaker first-order diffraction mode and higher zeroth-order diffraction mode. The slightly nonlinear optical response of the simulated grating efficiency, may contribute to the discrepancy between the height and optical reversibility (cf. Figures 2g and 3b).

CONCLUSION

Reversible shape memory (RSM) has been utilized to precisely replicate and control the shape of sub-μm features used in optical applications. This was determined by monitoring the diffraction efficiency as the patterned RSM substrate was subjected to heating−cooling cycles, within the range $T_p < T_m$. The maximum optical reversibility was determined to be 36% when T_p is near T_m = 56 °C. The diffraction intensity can be controlled and always returns within 10% of the original intensity, unless $T_p > T_m$. The approach presented for the fabrication of the gratings can be applied to more complicated optical nanostructures for use in optical analytical equipment such as active blazed gratings. Furthermore, monitoring optical scattering intensity was also found to be a viable way to observe melting and crystallization-induced roughness on the surface of semicrystalline polymers. Additional studies need to be performed to determine relationships between crystallite size and scattering effects.

ASSOCIATED CONTENT

Supporting Information

DMA tensile test of bulk poly(octylene adipate), grating height analysis methods, surface morphologies after complete melt, and scattering data of SMP gratings. The Supporting Information is available free of charge on the ACS Publications website at DOI: 10.1021/acsami.5b02688.

AUTHOR INFORMATION

Corresponding Authors

*Email: sergei@email.unc.edu.
*Email: rln@email.unc.edu.

Present Address

[‖]Department of Physics and Astronomy, The University of the South, Sewanee, TN 37383, United States

Author Contributions

[⊥]The manuscript was written through contributions of all authors. All authors have given approval to the final version of the manuscript. These authors contributed equally.

Funding

This material is based upon work funded by the National Science Foundation under award number DMR-1122483 and DMR-1243590.

Notes

The authors declare no competing financial interest.

REFERENCES

(1) Sinzinger, S.; Jahns, J. Microoptics for Optical Information Technology. In *Mircooptics*. Wiley-VCH: New York, 2003; pp 305−336
(2) Werber, A.; Zappe, H. Tunable Microfluidic Microlenses. *Appl. Opt.* **2005**, *44*, 3238−3245.
(3) Truxal, K.; Tung, S. C.; Kurabayashi, Y. C. A PDMS-on-Silicon Deformable Grating for Spectral Differentiation of Mixed Wavelength Signals. *Solid-State Sensor Actuat Microsystems Conf.* **2007**, 1087−1090.
(4) Ouyang, G.; Wang, K.; Henriksen, L.; Akram, M. N.; Chen, X. Y. A Novel Tunable Grating Fabricated with Viscoelastic Polymer (PDMS) and Conductive Polymer (PEDOT). *Sens. Actuators, A* **2010**, *158*, 313−319.
(5) Aschwanden, M.; Beck, M.; Stemmer, A. Diffractive Transmission Grating Tuned by Dielectric Elastomer Actuator. *IEEE Photonics Technol. Lett.* **2007**, *19*, 1090−1092.
(6) Xie, T. Recent Advances in Polymer Shape Memory. *Polymer* **2011**, *52*, 4985−5000.
(7) Havens, E.; Snyder, E. A.; Tong, T. H. Light-Activated Shape Memory Polymers and Associated Applications. *Proc. SPIE* **2005**, *5762*, 48−55.
(8) Xie, T. Tunable Polymer Multi-shape Memory Effect. *Nature* **2010**, *464*, 267−270.
(9) Behl, M.; Razzaq, M. Y.; Lendlein, A. Multifunctional Shape-Memory Polymers. *Adv. Mater.* **2010**, *22*, 3388−3410.
(10) Liu, Y.; Lv, H.; Lan, X.; Leng, J.; Du, S. Review of Electro-active Shape-Memory Polymer Composite. *Compos. Sci. Technol.* **2009**, *69*, 2064−2068.
(11) Chung, T.; Rorno-Uribe, A.; Mather, P. T. Two-way Reversible Shape Memory in a Semicrystalline Network. *Macromolecules* **2008**, *41*, 184−192.
(12) Pandini, S.; Passeraa, S.; Messorib, M.; Padernib, K.; Tosellic, M.; Gianoncellid, A.; Bontempid, E.; Riccòa, T. Two-Way Reversible Shape Memory Behaviour of Crosslinked Poly(epsilon-caprolactone). *Polymer* **2012**, *53*, 1915−1924.
(13) Westbrook, K. K.; Mather, P. T.; Parakh, V.; Dunn, M. L.; Ge, Q.; Lee, B. M.; Qi, H. J. Two-Way Reversible Shape memory Effects in a Free-Standing Polymer Composite. *Smar Mater. Struct* **2011**, *20*, 065010/1−9.
(14) Zhou, J.; Turner, S. A.; Brosnan, S. M.; Li, Q.; Carrillo, J. Y.; Nykypanchuk, D.; Gang, O.; Ashby, V. S.; Dobrynin, A. V.; Sheiko, S. S. Shapeshifting: Reversible Shape Memory in Semicrystalline Elastomers. *Macromolecules* **2014**, *47*, 1768−1776.
(15) Behl, M.; Kratz, K.; Noechel, U.; Sauter, T.; Lendlein, A. Temperature-Memory Polymer Actuators. *Proc. Natl. Acad. Sci. U.S.A.* **2013**, *110*, 12555−12559.
(16) Meng, Y.; Jiang, J.; Anthamatten, M. Shape Actuation via Internal Stress-Induced Crystallization of Dual-Cure Networks. *ACS Macro Lett.* **2015**, *4*, 115−118.
(17) Xu, H.; Yu, C.; Wang, S.; Malyarchuk, V.; Xie, T.; Rogers, J. A. Deformable, Programmable, and Shape-Memorizing Micro-Optics. *Adv. Funct. Mater.* **2013**, *23*, 3299−3309.
(18) Turner, S. A.; Zhou, J.; Sheiko, S. S.; Ashby, V. S. Switchable Micropatterned Surface Topographies Mediated by Reversible Shape Memory. *ACS Appl. Mater. Interfaces* **2014**, *6*, 8017−8021.

DOI: 10.1021/acsami.5b02688
ACS Appl. Mater. Interfaces 2015, 7, 14288−14293

(19) Espinha, A.; Serrano, M. C.; Blanco, Á.; López, C. Thermoresponsive Shape-Memory Photonic Nanostructures. *Adv. Opt. Mater.* **2014**, *2*, 516−521.
(20) Deka, B.; Sahu, P. P. Tooth-Shaped Grating-Assisted Structure for Compact Multimode Interference Coupler. *Appl. Opt.* **2011**, *50*, E193−199.
(21) Chang, C.-H.; Heilmann, R. K.; Fleming, R. C.; Carter, J.; Murphy, E.; Schattenburg, M. L.; Bailey, T. C.; Ekerdt, J. G.; Frankel, R. D.; Voisin, R. Fabrication Of Sawtooth Diffraction Gratings Using Nanoimprint Lithography. *J. Vac. Sci. Technol. B* **2003**, *21*, 2755−2759.
(22) Wang, J.; Shao, J.; Wang, S.; He, H.; Fan, Z. Antireflective Characteristics Of Triangular Shaped Gratings. *Chin. Opt. Lett.* **2005**, *3*, 497−499.
(23) Chang, C. L.; Acharya, G.; Savran, C. A. In Situ Assembled Diffraction Grating for Biomolecular Detection. *Appl. Phys. Lett.* **2007**, *90*, 233901/1−3.

DOI: 10.1021/acsami.5b02688
ACS Appl. Mater. Interfaces 2015, 7, 14288−14293